2021 International Conference on Advances in Electrical, Computing, Communication and Sustainable Technologies (ICAECT) | 978-1-7281-5791-7/20/$31.00 ©2021 IEEE | DOI: 10.1109/ICAECT49130.2021.9392631

Harmonics Mitigation Techniques in Grid Integrated PV based Microgrid: A Comparative Analysis

Avdhesh Kumar, Rachana Garg and Priya Mahajan

Department of Electrical Engineering, Delhi Technological University, Delhi, India
E-mail : iesavd@gmail.com, rachana16100@yahoo.co.in, priyamahajan.eed@gmail.com

Abstract : **With the increased penetration of photovoltaic (PV) based distributed generation (DG), power quality (PQ) at the point of common coupling (PCC) becomes a major concern mainly due to harmonics. Harmonics, generated by nonlinear loads in the system, are multiples of fundamental frequency. This paper presents the comparative analysis and discussion of various control techniques for VSC of a grid connected PV based micro grid to mitigate the harmonics. The mitigation of harmonics is achieved using control techniques viz. conventional and adaptive of reference generation. Simulation of the developed model is carried out on MATLAB/Simulink. Performance of the system is evaluated under IEEE-519 standard.**

Keywords—Power Quality (PQ), Power Factor Correction (PFC), Total Harmonic Distortions (THD), Voltage Source Converter (VSC)

I. INTRODUCTION

The increasing penetration of solar photovoltaic (SPV) system in utility grids, degrades power quality (PQ) at the point of common coupling (PCC) is becoming a major concern. Harmonics are generated either by nonlinear local loads or power electronics converter used in the PV based microgrid system [1-4]. The integration of PV system requires voltage source converter (VSC), switching of these converters generates harmonics at the output of microgrid. In the present study, harmonics generated due to local loads only are mitigated using different control algorithm of VSC [5]– [7]. In [8] authors have reported that a phase locked loop (PLL) is required to transform three phases to synchronous frame in SRF based control but sometimes it shows computational delay and also it has to be tuned preceding to its operation. In [9] authors reported that, in the implementation of IRPT and PBT, reference current is estimated using voltage and current of the PCC, so fluctuation in voltage will reflect in the reference current. While unit template is simplified form of adaptive LMS algorithm. Adaptive LMS suffer from fluctuations and less accuracy in estimating mean square error (MSE). In [10] authors reported that in the past few decades, adaptive control algorithms have been proposed for many applications. Among them, the least mean square (LMS) algorithm is the distinguished one. Due to its simplicity, conventional LMS adaptive control has been implemented widely but the performance is often unsatisfactory because of poor dynamic performance, due to compromise between tracking capability and accuracy in fixed step size.

In this paper, PV based microgrid has been integrated to grid. VSC is controlled using both conventional techniques viz. synchronous reference frame (SRF), instantaneous reactive power theory (IRPT), unit template, power balance theory (PBT) and adaptive Least mean square (LMS) technique [11]–[16]. MATLAB/Simulink software has been used for modelling and simulation of these algorithms. The efficacy of control algorithm of VSC shows the efficient operation of the grid integrated PV system. VSC maintain unity power factor at grid by supplying reactive power demand of load along-with active power. Further, in case of unbalanced loads, VSC maintain the grid currents balanced by supplying current to unbalance loads as per each phase requirement and also eliminates the harmonics in the grid current.

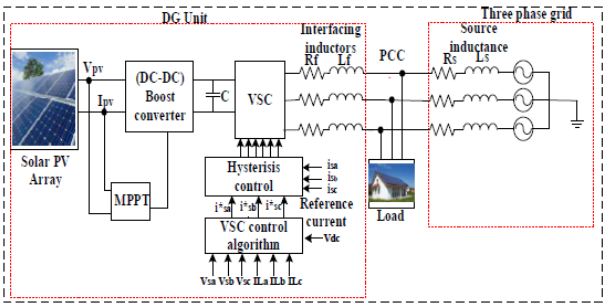

Fig.1 System configuration

II. SYSTEM CONFIGURATION

Fig. 1 depicts proposed system configuration. A 10.25kW SPV system has been integrated to grid. Various parameters of the system are given in the appendix. The proposed system consists of a SPV array, dc-dc (boost) converter, VSC and consumer loads. As power from PV array is not constant and changes with environmental conditions, therefore to get the maximum efficiency of SPV array, Perturb and observe MPPT algorithm is used [17]–[20]. DC link voltage obtained after boost converter is converted to ac voltage of required magnitude and frequency using VSC.

III. VSC CONTROL ALGORITHMS

A. SRF Control algorithm

Fig. 2 represents the block diagram of reference current estimation using SRF control algorithm under UPF mode of operation. Park's transformation has been used to convert load current components from synchronous rotating reference frame to d-q reference frame.

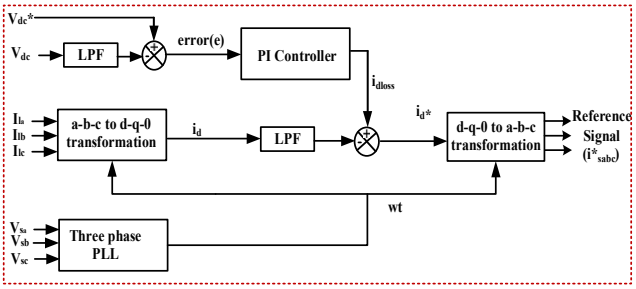

Fig. 2 SRF control algorithm

Three phase current in the a-b-c frame is transformed into d-q-0 frame by means of Park's conversion as given below:

$$\begin{bmatrix} i_d \\ i_q \\ i_0 \end{bmatrix} = \frac{2}{3}\begin{bmatrix} \cos w\,t & \cos(wt-120) & \cos(wt+120) \\ \sin wt & \sin(wt-120) & \sin(wt+120) \\ 1/2 & 1/2 & 1/2 \end{bmatrix}\begin{bmatrix} i_{la} \\ i_{lb} \\ i_{lc} \end{bmatrix} \quad (1)$$

PI controller, is used to maintain the voltage across dc link. fundamental active (i_d) and reactive (i_q) component of load currents are extracted by means of low pass filter. VSC must supply the reactive power demand of the load to operate the SRF algorithm in unity power factor mode. Reference reactive component (i_q^*) must be zero $(i_q^* = 0)$, to compensate the reactive demand of the load. While (i_d) is added with output of PI controller (i_{dloss}) in order to regulate the dc link voltage.

$$i_d^* = i_d + i_{dloss} \quad (2)$$

Further converting the reference signal from d-q frame to a-b-c by means of inverse parks transformation, provides reference current ($i_{sa}^*, i_{sb}^*, i_{sc}^*$).

Generated reference current (i^*_{sabc}) must be in same phase with grid voltage, using reverse Park's conversion as represented below, i^*_{sabc} are obtained:

$$\begin{bmatrix} i_{sa}^* \\ i_{sb}^* \\ i_{sc}^* \end{bmatrix} = \begin{bmatrix} cos\ wt & \sin wt & 1 \\ \cos(wt-120) & \sin(wt-120) & 1 \\ \cos(wt+120) & \sin(wt+120) & 1 \end{bmatrix}\begin{bmatrix} i_d \\ i_q \\ i_0 \end{bmatrix} \quad (3)$$

Reference current are compared with sensed grid current $(i_{sa}, i_{sb,} i_{sa})$ in hysteresis control and generate switching signals to operate VSC [8-12].

B. IRPT Theory of Inverter Control

Fig. 3 depicts the block diagram representation of IRPT control algorithm of reference current. In this control Clark's transformations are used to converts the PCC voltage and load current in to α-β frame respectively as given below:

$$\begin{bmatrix} v_\alpha \\ v_\beta \end{bmatrix} = \sqrt{(2/3)}\begin{bmatrix} 1 & -1/2 & -1/2 \\ 0 & \sqrt{3}/2 & -\sqrt{3}/2 \end{bmatrix}\begin{bmatrix} v_{sa} \\ v_{sb} \\ v_{sc} \end{bmatrix} \quad (4)$$

$$\begin{bmatrix} i_{L\alpha} \\ i_{L\beta} \end{bmatrix} = \sqrt{(2/3)}\begin{bmatrix} 1 & -1/2 & -1/2 \\ 0 & \sqrt{3}/2 & -\sqrt{3}/2 \end{bmatrix}\begin{bmatrix} i_{La} \\ i_{Lb} \\ i_{Lc} \end{bmatrix} \quad (5)$$

Instantaneous magnitude of active power (p_L) and reactive power (q_L) are computed using the equations (6) and (7) as given below:

$$p_L = v_\alpha i_{L\alpha} + v_\beta i_{L\beta} \quad (6)$$

$$q_L = v_\alpha i_{L\beta} + v_\beta i_{L\alpha} \quad (7)$$

$$\begin{bmatrix} p_L \\ q_L \end{bmatrix} = \begin{bmatrix} \overline{p_L} & +\widetilde{p_L} \\ \overline{q_L} & +\widetilde{p_L} \end{bmatrix} \quad (8)$$

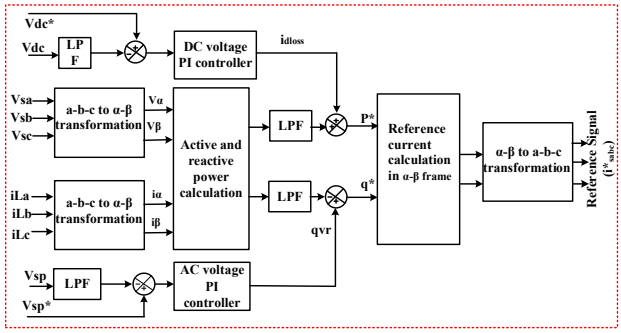

Fig. 3 IRPT control algorithm

Computed power contains both dc and ac component. To filter out the fundamental power components, low pass filters are used. Reference active and reactive component of power is estimated using Eq. given below:

$$p^* = \overline{p_L} + p_{loss} \quad (9)$$

$$q^* = \overline{q_L} + q_{vr} \quad (10)$$

Reference current ($i_{sa}^*, i_{sb}^*, i_{sc}^*$) is estimated as given below:

$$\begin{bmatrix} i_{sa}^* \\ i_{sb}^* \\ i_{sc}^* \end{bmatrix} = \sqrt{(2/3)}\begin{bmatrix} 1 & 0 \\ -1/2 & \sqrt{3}/2 \\ -1/2 & -\sqrt{3}/2 \end{bmatrix}\begin{pmatrix} v_\alpha & v_\beta \\ -v_\beta & v_\alpha \end{pmatrix}^{-1}\begin{bmatrix} p^* \\ q^* \end{bmatrix} \quad (11)$$

In PFC mode reference reactive power component (q^*) should be zero to maintain the grid at unity power factor. Reference current are compared with sensed grid current $(i_{sa}, i_{sb,} i_{sa})$ in hysteresis control and generate switching signals to operate VSC [13-15].

C. Unit template Control algorithm

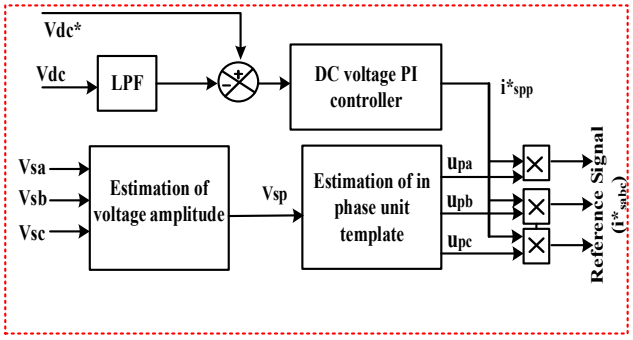

Fig.4 Unit template control algorithm

Unit template control algorithm of VSC for estimating the reference currents shown in Fig.4.The unit template is a simple VSC control technique for estimating the reference current. This control algorithm can be made flexible and it can be modified either for PFC or voltage regulation at PCC. The unit template control algorithm in PFC mode of operation is performed to estimate reference current as shown in the fig. 4. PCC voltage and DC bus voltage of VSC are used for implementing this control algorithm. A band-pass filter (BPF) can be used to remove distortion in sampled PCC voltages in real time implementation. Assume that after filtering the PCC voltage signal is (v_{sa}, v_{sb}, v_{sc}). Peak amplitude of PCC voltage is calculated as:

$$v_{sp} = \sqrt{\frac{2}{3}(v_{sa}^2 + v_{sb}^2 + v_{sc}^2)} \quad (12)$$

The in-phase unit voltages template ($\mathcal{U}_{pa}, \mathcal{U}_{pb}, \mathcal{U}_{pc}$) can be calculated using phase voltages ($\mathcal{V}_{sa}, \mathcal{V}_{sb}, \mathcal{V}_{sc}$) with peak amplitude($\mathcal{V}_{sp}$) as follows:

$$\mathcal{U}_{pa} = \frac{\mathcal{V}_{sa}}{\mathcal{V}_{sp}}, \mathcal{U}_{pb} = \frac{\mathcal{V}_{sb}}{\mathcal{V}_{sp}}, \mathcal{U}_{pc} = \frac{\mathcal{V}_{sc}}{\mathcal{V}_{sp}} \quad (13)$$

Further, error in DC link voltage is compensated using PI controller. Output of PI controller is considered as amplitude of reference current (i^*_{spp}) . Amplitude of reference current(i^*_{spp}) are multiplied by in- phase unit template to get reference current ($i^*_{sa}, i^*_{sb}, i^*_{sc}$) as given below:

$$i^*_{sa} = i^*_{spp}\mathcal{U}_{sa}, i^*_{sb} = i^*_{spp}\mathcal{U}_{sb}, i^*_{sc} = i^*_{spp}\mathcal{U}_{sc} \quad (14)$$

Reference current ($i^*_{sa}, i^*_{sb}, i^*_{sc}$) are compared with sensed grid current (i_{sa}, i_{sb}, i_{sa}) in hysteresis control and generate switching signals to operate VSC.

D. Power balance theory control algorithm

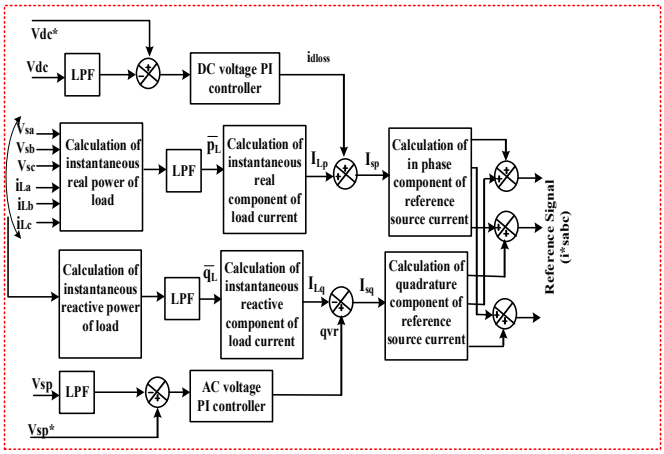

Fig.5 Power balance theory-based control algorithm

Fig. 5 depicts the block diagram representation of PBT control algorithm for generation of reference current. In this control, instantaneous power consumed by the loads can be utilized to extract of fundamental components of load currents. This algorithm sense the load currents, DC bus voltage, PCC voltage and grid current of proposed system. DC link PI controller output is added with fundamental active power component of load current as in eqn. (17) to regulate DC link voltage and to estimate the fundamental active power component of reference supply current. Eqn. (18) and (20) are used to compute instantaneous power (active and reactive) component of reference currents. Further to get reference current, in phase and quadrature reference current added together by taking respective phases.

The peak amplitude of voltage ($\mathcal{V}_t$)of grid voltage, can be calculated by:

$$\mathcal{V}_t = \sqrt{\frac{2}{3}(\mathcal{V}_{sa}^2 + \mathcal{V}_{sb}^2 + \mathcal{V}_{sc}^2)} \quad (15)$$

The in-phase unit template voltages ($\mathcal{U}_{pa}, \mathcal{U}_{pb}, \mathcal{U}_{pc}$) can be calculated from phase voltages ($\mathcal{V}_{sa}, \mathcal{V}_{sb}, \mathcal{V}_{sc}$) and peak amplitude ($\mathcal{V}_t$) as follows:

$$\mathcal{U}_{pa} = \frac{\mathcal{V}_{sa}}{\mathcal{V}_t}, \mathcal{U}_{pb} = \frac{\mathcal{V}_{sb}}{\mathcal{V}_t}, \mathcal{U}_{pc} = \frac{\mathcal{V}_{sc}}{\mathcal{V}_t} \quad (16)$$

The reactive/orthogonal/quadrature unit templates ($\mathcal{U}_{qa}, \mathcal{U}_{qb}, \mathcal{U}_{qc}$) can be obtained from in phase unit template voltages as follows:

$$u_{qa} = -\frac{u_{pb}}{\sqrt{3}} + \frac{u_{pc}}{\sqrt{3}}, u_{qb} = \frac{\sqrt{3}\,u_{pa}}{2} + \frac{(u_{pb}-u_{pc})}{2\sqrt{3}}, \quad u_{qc} = -\frac{\sqrt{3}\,u_{pa}}{2} + \frac{(u_{pb}-u_{pc})}{2\sqrt{3}} \quad (17)$$

The instantaneous active and reactive powers of the load are calculated as:

$$p_L = v_{sa}i_{La} + v_{sb}i_{Lb} + v_{sc}i_{Lc} = \overline{p_L} + \widetilde{p_L} \quad (18)$$

$$q_L = \sqrt{(1/3)[(v_{sa}-v_{sb})i_{Lc} + (v_{sb}-v_{sc})i_{La} + (v_{sc}-v_{sb})i_{Lb}]} = \overline{q_L} + \widetilde{q_L} \quad (19)$$

Fundamental power (active and reactive) component of the loads are extracted by means of LPFs from instantaneous powers.

Amplitude of active power fundamental component of load currents is estimated from average load power.

$$I_{Lp} = (2/3)(\frac{\overline{p_L}}{\mathcal{V}_{sp}}) \quad (20)$$

Moreover, amplitude of reactive power fundamental component of load currents is estimated from average load power:

$$I_{Lq} = (2/3)(\frac{\overline{q_L}}{\mathcal{V}_{sp}}) \quad (21)$$

Output of the DC voltage PI controller(i_{dloss}) of the proposed system is added with fundamental active power component of load currents (I_{Lp}) to estimate amplitude of the active power component of reference supply currents as given below:

$$I_{sp} = i_{dloss} + I_{Lp} \quad (22)$$

In-phase unit templates of respective phases is multiplied by amplitude component of the active power (I_{sp}) of reference supply current. The instantaneous fundamental active power component (in-phase) of reference supply currents($i^*_{spa}, i^*_{spb}i^*_{spc}$) are given as:

$$i^*_{sap} = I_{sp} * \mathcal{U}_{pa};\ i^*_{sbp} = I_{sp} * \mathcal{U}_{pb};\ i^*_{scp} = I_{sp} * \mathcal{U}_{pc} \quad (23)$$

Similarly, amplitude estimation of fundamental component of reactive power (I_{sq}) of reference supply currents is estimated is given in the eqn. below:

$$I_{sq} = q_{vr} - I_{Lq} \quad (24)$$

Further to get instantaneous values of the fundamental reactive power component of reference supply currents, amplitude of fundamental reactive component is multiplied by quadrature unit templates. Instantaneous quadrature reference current ($i^*_{sqa}, i^*_{sqb}, i^*_{sqc}$) are given as:

$$i^*_{saq} = I_{sq} * \mathcal{U}_{qa};\ i^*_{sbq} = I_{sq} * \mathcal{U}_{qb}; i^*_{scq} = I_{sq} * \mathcal{U}_{qc} \quad (25)$$

The adding in-phase and quadrature reference supply current will give the instantaneous fundamental reference supply currents as given:

$$i^*_{sa} = i^*_{sap} + i^*_{saq}, i^*_{sb} = i^*_{sbp} + i^*_{sbq}, i^*_{sc} = i^*_{scp} + i^*_{scq} \quad (26)$$

Further reference current ($i^*_{sa}, i^*_{sb}, i^*_{sc}$) are compared with sensed grid current (i_{sa}, i_{sb}, i_{sa}) in hysteresis control and generate switching signals to operate VSC.

E. Adaptive LMS Control algorithm

LMS control technique computes the reference currents to generate pulses for VSC conduction as demonstrated in Fig. 6. Control algorithm is described as follows:

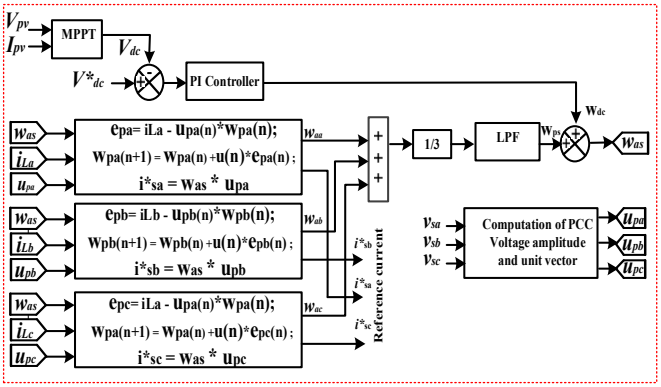

Fig. 6 Adaptive LMS Control algorithm

Estimation of in phase and unite templates of voltages

The peak amplitude of voltage ($\mathcal{V}_t$) of grid voltage, which can be calculated by:

$$\mathcal{V}_t = \sqrt{\frac{2}{3}(\mathcal{V}_{sa}^2 + \mathcal{V}_{sb}^2 + \mathcal{V}_{sc}^2)} \quad (27)$$

The in-phase unit voltages template ($\mathcal{U}_{pa}, \mathcal{U}_{pb}, \mathcal{U}_{pc}$) can be calculated by the relation of phase voltages ($\mathcal{V}_{sa}, \mathcal{V}_{sb}, \mathcal{V}_{sc}$) with peak amplitude ($\mathcal{V}_t$) voltages as follows [20]:

$$\mathcal{U}_{pa} = \frac{\mathcal{V}_{sa}}{\mathcal{V}_t}, \mathcal{U}_{pb} = \frac{\mathcal{V}_{sb}}{\mathcal{V}_t}, \mathcal{U}_{pc} = \frac{\mathcal{V}_{sc}}{\mathcal{V}_t} \quad (28)$$

Estimation of active weight using LMS control algorithm

Error in active component of load current in each phase ($e_{pa}; e_{pb}; e_{pc}$) at n_{th} instant is estimated as using in-phase unit template ($\mathcal{U}_{pa}, \mathcal{U}_{pb}, \mathcal{U}_{pc}$) and active load current component ($w_{pa}; w_{pc}; w_{pc}$)as follows:

$$e_{pa}(n) = i_{La}(n) - u_{pa} * w_{pa}(n) \quad (29)$$

$$e_{pb}(n) = i_{Lb}(n) - u_{pb} * w_{pb}(n) \quad (30)$$

$$e_{pc}(n) = i_{Lc}(n) - u_{pc} * w_{pc}(n) \quad (31)$$

The fundamental active weights w_{pa}, w_{pb}, w_{pc} at (n+1) instant be computed as:

$$w_{pa}(n+1) = w_{pa}(n) + \mu(n) * e_{pa}(n) \quad (32)$$

$$w_{pb}(n+1) = w_{pb}(n) + \mu(n) * e_{pb}(n) \quad (33)$$

$$w_{pc}(n+1) = w_{pc}(n) + \mu(n) * e_{pc}(n) \quad (34)$$

The average fundamental active weight components can be computed as:

$$w_{lp} = \frac{(w_{pa}+w_{pb}+w_{pc})}{3} \quad (35)$$

The sensed voltage of dc-link (V_{dc}) is compared with reference dc bus voltage (V_{dc}^*) to estimate error in DC link voltage and compensated using proportional integral (PI) controller. The output of the controller is dc loss weight (w_{dc}).

The total active weight (w_{ps}) component of the supply reference current is given by:

$$w_{ps} = w_{lp} + w_{dc} \quad (36)$$

The active in-phase reference supply current can be evaluated as:

$$i_{sa}^* = w_{ps}\mathcal{U}_{pa}, i_{sb}^* = w_{ps}\mathcal{U}_{pb}, i_{sc}^* = w_{ps}\mathcal{U}_{pc} \quad (37)$$

Generation of switching signal for VSC

Reference current ($i_{sa}^*, i_{sb}^*, i_{sc}^*$) are compared with sensed grid current (i_{sa}, i_{sb}, i_{sa}) in hysteresis control and generate switching signals to operate VSC.

IV. RESULTS AND DISCUSSIONS

To analyze the efficacy of various control algorithms under nonlinear load, a bridge rectifier has been considered with RL load (R=100 Ω, L=100 mH). Further, to create the unbalance in the load, one phase is kept open from 0.15 to 0.25 seconds. Proposed system is supposed to be working at standard test condition (1000w/m^2, 25^{0}C). Proposed system is conducted in PFC mode of operation.

A. Performance of Various Control algorithm

Simulation results using various control algorithms under nonlinear(balance/unbalance) load are given in the Fig.7. To impose the unbalance between 0.15 to 0.25 second one phase is kept open. It can be seen from Fig. 7 that all the algorithms are efficient in maintaining the grid current sinusoidal and balanced for the unbalance load current between 0.15 to 0.25 sec. Fig 8 shows the grid current waveform and THD. It can be seen from Fig 8 (a) and table I, that load current THD is 29.28% while grid current THD is well within the IEEE standard-519.

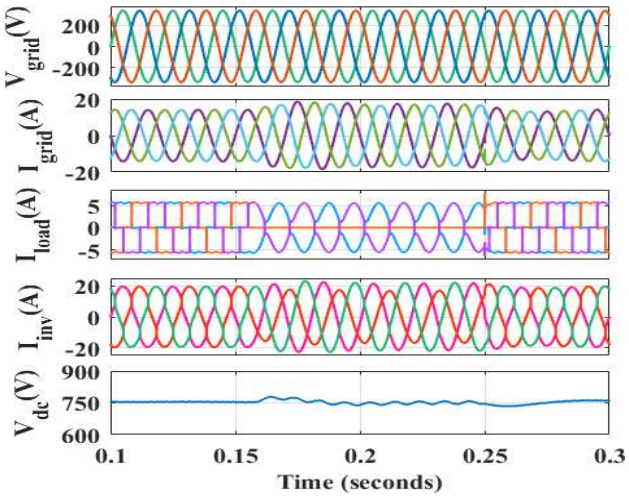

(a) Grid integrated microgrid under SRF control

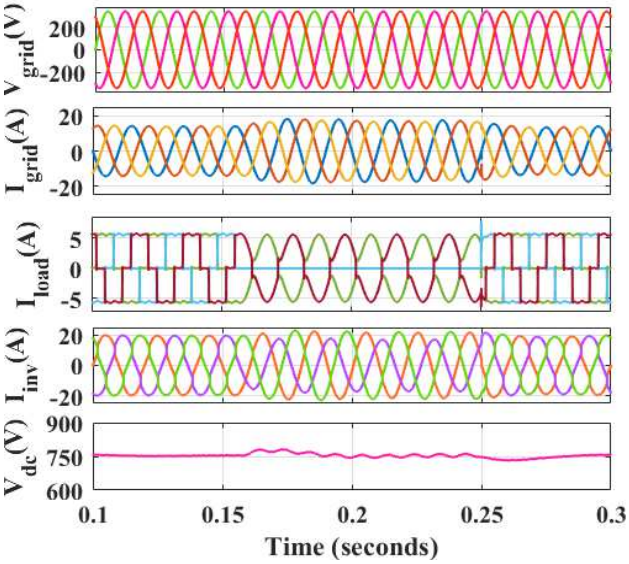

(b) grid integrated microgrid under IRPT control

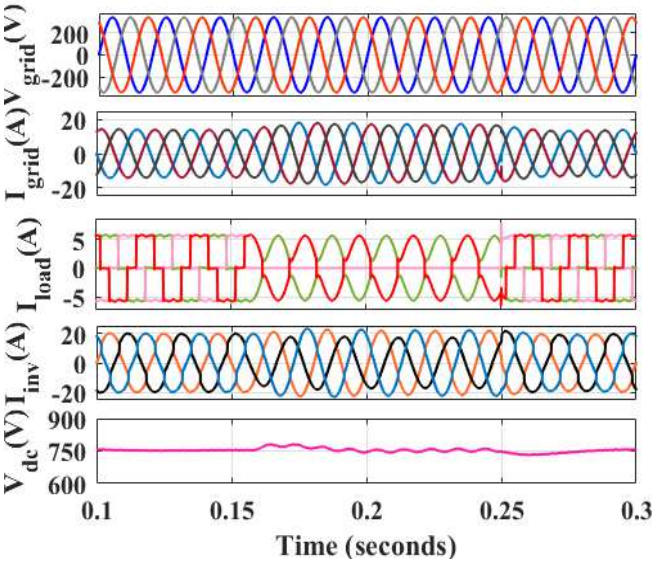

(c) Grid integrated microgrid under unit template control

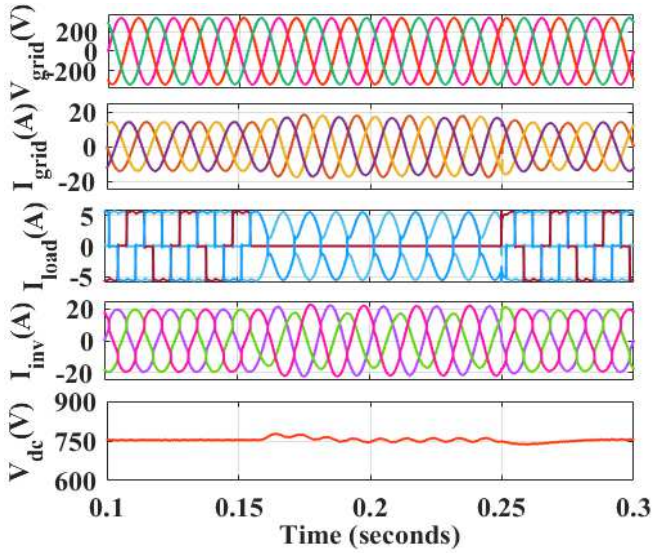

(d) Grid integrated microgrid under PBT control

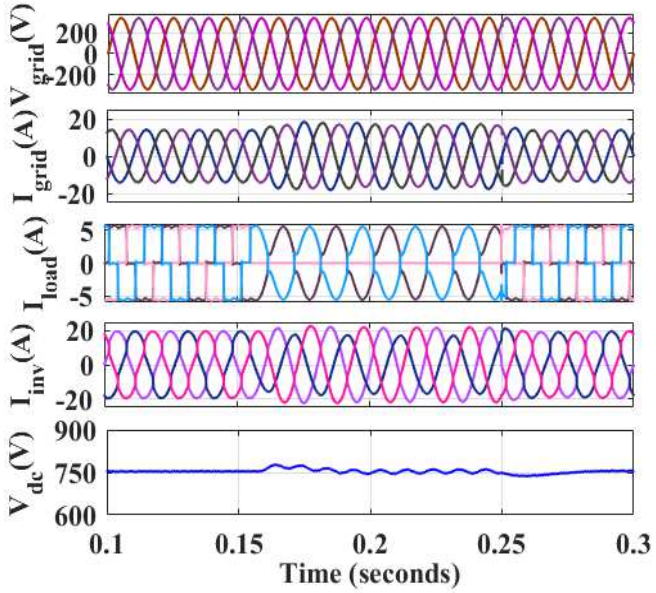

(e) Grid integrated microgrid under adaptive LMS control

Fig. 7(a), (b), (c), (d) and (e)

B. Grid curent waveform and THD under nonlinear load

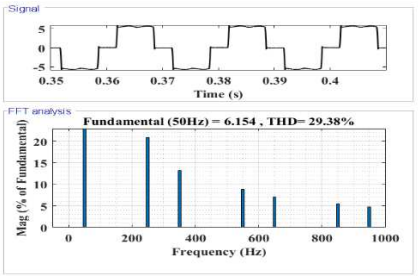

(a) Grid current waveform and THD before compensation

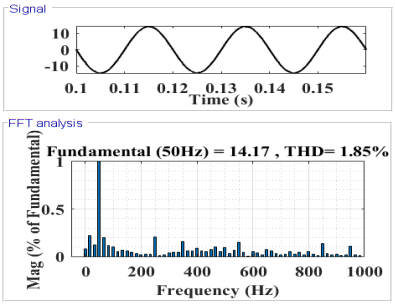

(b) Grid current waveform and THD after compensation using SRF control

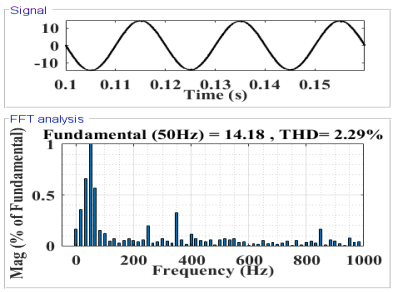

(c) Grid current waveform and THD after compensation using IRPT control

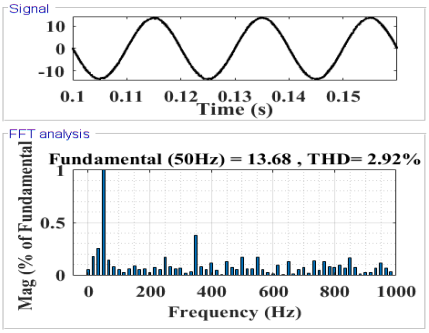

(d) Grid current waveform and THD after compensation using unit template control

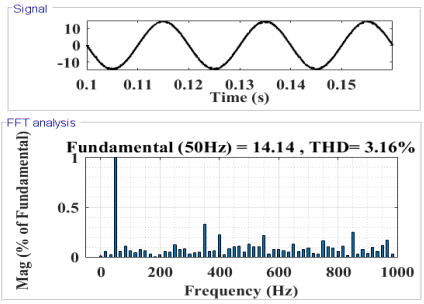

(e) Grid current waveform and THD after compensation using PBT control

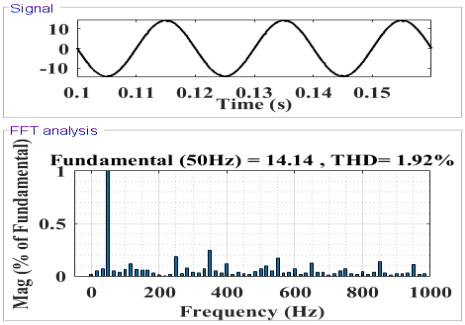

(f) Grid current waveform and THD after compensation using LMS control

Fig.8(a), (b), (c), (d), (e) and (f)

It can be seen from table I, that harmonics in grid current is minimum in case of SRF, while adaptive LMS provides slightly higher than SRF and less than other algorithm. Implementation of adaptive LMS is simplest than other, but advance type of adaptive LMS control can offer the best performance towards harmonics mitigation.

TABLE I.

S.N.	THD in grid current	
	Control algorithms	*THD*
1	SRF	1.85
2	IRPT	2.29
3	Unit template	2.92
4	PBT	3.16
5	LMS	1.92

Conclusion

In this paper, different conventional and adaptive LMS control algorithms have been implemented for controlling the PV base microgrid. The performance of the control algorithm is tested under nonlinear (balanced/unbalanced) load at STC. It has been observed that under different control, of VSC, microgrid operation is efficient and THD in grid current is maintained within limit along with UPF operation. Comparative analysis of different control algorithm under PV grid integration depicts that harmonics in grid current is minimum i.e. 1.85% in case of SRF while adaptive LMS offers minimum complexity in implementation and provides almost similar 1.92% THD in the grid current.

REFERENCES

[1] N. Beniwal, I. Hussain, and B. Singh, "A second-order volterra filter based control of SPV-DSTATCOM system to achieve Lyapunov's stability," *2016 IEEE 7th Power India Int. Conf.*, pp. 1–5, 2016, doi: 10.1109/POWERI.2016.8077292.

[2] B. Singh, P. Jayaprakash, D. P. Kothari, A. Chandra, and K. Al Haddad, "Comprehensive study of dstatcom configurations," *IEEE Trans. Ind. Informatics*, vol. 10, no. 2, pp. 854–870, 2014, doi: 10.1109/TII.2014.2308437.

[3] T. A. Youssef and O. Mohammed, "Adaptive SRF-PLL with reconfigurable controller for Microgrid in grid-connected and stand-alone modes," IEEE Power Energy Soc. Gen. Meet., pp. 1–5, 2013, doi: 10.1109/PESMG.2013.6673028.

[4] S. R. Arya, B. Singh, R. Niwas, A. Chandra, and K. Al-Haddad, "Power Quality Enhancement Using DSTATCOM in Distributed Power Generation System," *IEEE Trans. Ind. Appl.*, vol. 52, no. 6, pp. 5203–5212, 2016, doi: 10.1109/TIA.2016.2600644.

[5] B. Singh, A. Chandra, and K. Al-haddad, "Power Quality Problems and Mitigation Techniques" Wiley Online Library, vol. 9781118922. 2015.

[6] S. K. Patel, S. R. Arya, and R. Maurya, "Optimal Step LMS-Based Control Algorithm for DSTATCOM in Distribution System," *Electr. Power Components Syst.*, vol. 47, no. 8, pp. 704–720, 2019, doi: 10.1080/15325008.2019.1602797.

[7] S. Kumar, A. K. Verma, I. Hussain, and B. Singh, "Performance of grid interfaced solar PV system under variable solar intensity," *India Int. Conf. Power Electron. IICPE*, vol. 2015-May, pp. 1–6, 2015, doi: 10.1109/IICPE.2014.7115797.

[8] N. Beniwal, I. Hussain, and B. Singh, "Implementation of the DSTATCOM with an i-PNLMS-Based Control Algorithm under Abnormal Grid Conditions," *IEEE Trans. Ind. Appl.*, vol. 54, no. 6, pp. 5640–5648, 2018, doi: 10.1109/TIA.2018.2846739.

[9] N. Beniwal, I. Hussain, and B. Singh, "Second-order volterra-filter-based control of a solar PV-DSTATCOM system to achieve lyapunov's stability," *IEEE Trans. Ind. Appl.*, vol. 55, no. 1, pp. 670–679, 2019, doi: 10.1109/TIA.2018.2867324.

[10] Z. Li, D. Li, X. Xu, and J. Zhang, "New normalized LMS adaptive filter with a variable regularization factor," *J. Syst. Eng. Electron.*, vol. 30, no. 2, pp. 259–269, 2019, doi: 10.21629/JSEE.2019.02.05.

[11] B. Singh, A. Chandra, and K. Al-haddad, "*Power Quality Problems and Mitigation Techniques" Wiley Online Library*, vol. 9781118922. 2015.

[12] S. R. Arya, B. Singh, A. Chandra, and K. Ai-Haddad, "Control of DSTATCOM using adjustable step least mean square control algorithm," *2012 IEEE 5th Power India Conf. PICONF 2012*, vol. 2, no. 1, pp. 1–6, 2012, doi: 10.1109/PowerI.2012.6479508.

[13] R. Garg and P. Mahajan, "Performance Analysis of Grid Integrated PV System using SRF and IRPT Control", 1st International Conference on Signal Processing, VLSI and Communication Engineering (ICSPVCE), 28-30 March 2019, DOI: 10.1109/ICSPVCE46182.2019.9092869.

[14] B. Singh, D. T. Shahani, and A. K. Verma, "Power balance theory based control of grid interfaced solar photovoltaic power generating system with improved power quality," *PEDES 2012 - IEEE Int. Conf. Power Electron. Drives Energy Syst.*, 2012, doi: 10.1109/PEDES.2012.6484359.

[15] P. K. Barik, G. Shankar, and P. K. Sahoo, "Power quality assessment of microgrid using fuzzy controller aided modified SRF based designed SAPF," *Int. Trans. Electr. Energy Syst.*, 2019, doi: 10.1002/2050-7038.12289.

[16] M. Esmaeili, H. Shayeghi, K. Valipour, A. Safari, and F. Sedaghati, "Power quality improvement of multimicrogrid using improved custom power device called as distributed power condition controller," *Int. Trans. Electr. Energy Syst.*, vol. 30, no. 3, pp. 1–16, 2020, doi: 10.1002/2050-7038.12259.

[17] P. Verma, R. Garg, and P. Mahajan, "Asymmetrical interval type-2 fuzzy logic control based MPPT tuning for PV system under partial shading condition," *ISA Trans.*, no. January, 2020, doi: 10.1016/j.isatra.2020.01.009.

[18] S. K. Kollimalla and M. K. Mishra, "Variable perturbation size adaptive P&O MPPT algorithm for sudden changes in irradiance," *IEEE Trans. Sustain. Energy*, vol. 5, no. 3, pp. 718–728, 2014, doi: 10.1109/TSTE.2014.2300162.

[19] J. Mishra, "Performance Comparison of P & O and INC MPPT Algorithm for a Stand-alone PV System," no. 1, pp. 1–5, 2019.

[20] N. Femia, G. Petrone, G. Spagnuolo, and M. Vitelli, "A technique for improving P&O MPPT performances of double-stage grid-connected photovoltaic systems," *IEEE Trans. Ind. Electron.*, vol. 56, no. 11, pp. 4473–4482, 2009, doi: 10.1109/TIE.2009.2029589.

Appendix

Simulation Parameters of the system: Grid voltages: 415 V, frequency (f): 50 Hz, Line impedances (R_s, L_s): 0.01Ω, 0.1mH, Interfacing inductor (Lf): 7mH, $V_{dc(ref.)}$: 750 V; sampling time T_s = 5.5μs

Solar PV parameters: nominal power 10.25 kW, nominal voltage at MPP: 410V, nominal current: 25 A,

DC-DC (boost) converter parameters**:** Duty cycle (D): 0.43, Switching frequency (f_s): 10 kHz**,** Inductor (L): 0.5mH, Capacitor (C): 1000μF,

Nonlinear load: bridge rectifier R=100Ω, L=100mH (unbalancing imposed between 0.15 to 0.25sec)